

Accepted Manuscript

Neuronal Development and Onset of Electrical Activity in the Human Enteric Nervous System

Conor J. McCann, Maria M. Alves, Erwin Brosens, Dipa Natarajan, Silvia Perin, Chey Chapman, Robert M. Hofstra, Alan J. Burns, Nikhil Thapar

PII: S0016-5085(18)35435-0
DOI: <https://doi.org/10.1053/j.gastro.2018.12.020>
Reference: YGAST 62339

To appear in: *Gastroenterology*
Accepted Date: 24 December 2018

Please cite this article as: McCann CJ, Alves MM, Brosens E, Natarajan D, Perin S, Chapman C, Hofstra RM, Burns AJ, Thapar N, Neuronal Development and Onset of Electrical Activity in the Human Enteric Nervous System, *Gastroenterology* (2019), doi: <https://doi.org/10.1053/j.gastro.2018.12.020>.

This is a PDF file of an unedited manuscript that has been accepted for publication. As a service to our customers we are providing this early version of the manuscript. The manuscript will undergo copyediting, typesetting, and review of the resulting proof before it is published in its final form. Please note that during the production process errors may be discovered which could affect the content, and all legal disclaimers that apply to the journal pertain.



Neuronal Development and Onset of Electrical Activity in the Human Enteric
Nervous System

Conor J. McCann,¹ Maria M. Alves,² Erwin Brosens,² Dipa Natarajan,¹ Silvia Perin,¹
Chey Chapman,¹ Robert M. Hofstra,^{1,2} Alan J. Burns^{1,2} & Nikhil Thapar^{1,3}

¹Stem Cells and Regenerative Medicine, UCL Great Ormond Street Institute of Child
Health, 30 Guilford Street, London, WC1N, UK. ²Department of Clinical Genetics,
Erasmus University Medical Center, Rotterdam, The Netherlands. ³Department of
Gastroenterology, Great Ormond Street Hospital, London, UK

Correspondence: Nikhil Thapar

Stem Cells and Regenerative Medicine, UCL Great Ormond Street Institute of Child
Health, 30 Guilford Street, London, WC1N 1EH, UK. Tel: +442079052711
Fax: +442079052953. email: n.thapar@ucl.ac.uk

Disclosures: No conflicts of interest exist for this study.

Author contributions: C.J.M., M.M.A., E.B., D.N., S.P. & C.C. acquired and
interpreted data. R.M.H., A.J.B. and N.T. interpreted data and obtained funding.
C.J.M., R.M.H., A.J.B. and N.T. contributed to study concept and design, and
drafted the manuscript.

Abbreviations

AP - Action Potential

BSA - Bovine Serum Albumin

ChAT - Choline acetyltransferase

E - Embryonic day

ENCC - Enteric neural crest cell

ENS - Enteric nervous system

EW - Embryonic week

FACS - Fluorescence activated cell sorting

GI – Gastrointestinal

Hex - Hexamethonium

ICC - Interstitial cells of Cajal

nNOS - Neuronal nitric oxide synthase

Sub P - Substance P

SYP - Synaptophysin

TTX - Tetrodotoxin

VACht - Vesicular acetylcholine transporter

VIP - Vasoactive intestinal peptide

Data Availability

The data that support the findings of this study are available from the corresponding author upon reasonable request. Transcript profiling: RNA-seq data is deposited in the Gene Expression Omnibus database (<https://www.ncbi.nlm.nih.gov/geo/>) under the accession number GSE111307.

Grant support

NT is supported by Great Ormond Street Hospital Children's Charity (GOSHCC - V1258). This work was funded through a GOSHCC grant (W1018C) awarded to NT (Principal Investigator) and AJB (Co-Investigator). CM is supported by Guts UK (Derek Butler Fellowship).

Acknowledgements

The human embryonic and fetal material was provided by the Joint MRC/Wellcome Trust grant# 099175/Z/12/Z Human Developmental Biology Resource (<http://hdbr.org>).

The authors would like to acknowledge the NIHR Great Ormond Street Hospital Biomedical Research Centre which supports all research at Great Ormond Street Hospital NHS Foundation Trust and UCL Great Ormond Street Institute of Child Health. The views expressed are those of the author(s) and not necessarily those of the NHS, the NIHR or the Department of Health.

Abstract:

Background & Aims: The enteric nervous system (ENS) is the largest branch of the peripheral nervous system, comprising complex networks of neurons and glia, which are present throughout the gastrointestinal (GI) tract. Although development of a fully functional ENS is required for GI motility, little is known about the ontogeny of ENS function in humans. We studied the development of neuronal subtypes and the emergence of evoked electrical activity within the developing human ENS.

Methods: Human fetal gut samples (obtained via the MRC-Wellcome Trust Human Developmental Biology Resource-UK) were characterized by immunohistochemistry, calcium imaging, RNAseq, and quantitative real-time PCR analyses.

Results: Human fetal colon samples have dense neuronal networks at the level of the myenteric plexus by embryonic week (EW) 12, with expression of excitatory neurotransmitter and synaptic markers. By contrast, markers of inhibitory neurotransmitters were not observed until EW14. Electrical train stimulation of internodal strands did not evoke activity within the ENS of EW12 or EW14 tissues. However, compound calcium activation was observed at EW16, which was blocked by the addition of 1 μ M tetrodotoxin. Expression analyses showed this activity was coincident with increases in expression of genes encoding proteins involved in neurotransmission and action potential generation.

Conclusions: In analyses of human fetal intestinal samples, we followed development of neuronal diversity, electrical excitability, and network formation in the ENS. These processes are required to establish the functional enteric circuitry. Further studies

could increase our understanding of the pathogenesis of a range of congenital enteric neuropathies.

Keywords: fetus, embryology, intestine, foetal

ACCEPTED MANUSCRIPT

Introduction

The enteric nervous system (ENS), the largest branch of the peripheral nervous system, is comprised of complex networks of neurons and glia, which are present throughout the gastrointestinal tract.¹ The ENS is derived primarily from vagal neural crest cells,² which enter the foregut at embryonic day 9 (E9) in mice and migrate in a rostrocaudal fashion to colonise the entirety of the developing gut by E14.^{3,4} In avian and mouse models, a smaller population of sacral neural crest-derived cells has also been shown to contribute to the developing ENS in the terminal hindgut.^{2,5} During ENS development, enteric neural crest cells (ENCC) proliferate and migrate extensively in a highly complex manner, with elongation of migratory chains of ENCC throughout the gut, including trans-mesenteric migration pathways that have been demonstrated in the mouse.⁶ Recent murine work has proposed that topographically, the ENS is built from parallel, overlapping columns of clonally derived ENCC. Such topographical organization relies upon residual founder ENCC at the level of the myenteric plexus, which give rise to progeny that extend through the width of the gut wall and are arranged along the serosa-mucosa axis.⁷ Previous work has demonstrated the spatio-temporal development of neuronal subtypes in the mouse gut, with the appearance of nitrergic neuronal nitric oxide synthase (nNOS) expressing neurons at approximately E12.5,⁸ and subsequent development of cholinergic neurons expressing choline acetyltransferase (ChAT) at E14.5.⁹ Furthermore, physiological studies in the murine colon have demonstrated the emergence of spontaneous calcium transients within ENCC at the migratory wavefront at E12.5,¹⁰ and the emergence of induced electrical activity in colonic networks at approximately E15.5.¹¹

Despite these significant advances in our knowledge regarding the

development of the ENS in animal models, insight to many of these developmental milestones in the human ENS is lacking. Previous work has provided evidence of similar rostrocaudal colonization in the human gut, whereby ENCC enter the foregut at embryonic week (EW) 4 and migrate in an oro-anal fashion to fully colonize the length of the gut by EW7.^{12, 13} Following ENCC colonization, development and maturation of the *tunica muscularis* occurs, with rostrocaudal differentiation of the smooth muscle layers and development of interstitial cell of Cajal (ICC) networks.¹³ Hence, at approximately EW11 the human colon has adopted an anatomically “mature” phenotype. These studies established the critical time frame for colonization and development of the ENS in human fetal gut tissues. However, there is a paucity of evidence regarding the development of neuronal subtypes or of coordinated electrical activity within the human ENS, which are vital processes for the establishment of the normal functional circuitry that underpins neuromuscular function of the gastrointestinal tract.

Here, we show that the spatio-temporal development of multiple enteric neuronal subtypes in the human fetal colon occurs within the early second trimester period. We further demonstrate the onset of coordinated neural activity within the human enteric neural network and show that this activity is coincident with increases in expression of various genes involved in neurotransmission and action potential generation. Thus, we propose that the period from late first trimester to early second trimester is crucial for the development of a repertoire of enteric neural subtypes and to the establishment of a functional ENS.

Methods

Human samples

Human fetal colonic samples were obtained via the Joint MRC/Wellcome Trust Human Developmental Biology Resource (HDBR) under informed ethical consent with Research Tissue Bank ethical approval (08/H0712/34+5 and 08/H0906/21+5).

Immunohistochemistry

Immunohistochemistry was performed on fetal wholemount colonic segments and cryostat sections as previously described¹⁴ (see Supplementary Materials and Methods) using the primary and secondary antibodies listed in Supplementary Tables 2&3 respectively.

Calcium imaging

Fetal intestinal samples were obtained as previously described and calcium imaging was performed as previously published.¹⁵ Following tissue excision and preparation (see Supplementary Materials and Methods) electrical train stimulation (2 s, 20 Hz of 300 μ s electrical pulses; Electronic stimulator 1001, AD instruments) was applied via a platinum/iridium electrode and images were collected using OptoFluor software (Cairn Research Limited).

RNA extraction and sequencing

Total RNA from the hindgut of one individual embryo from each time-point (EW12, EW14 and EW16), was extracted using the RNeasy kit and protocol (Qiagen, Venlo, The Netherlands). RNA quantity and quality was determined using the Lab-on-Chip RNA 6000 Nano (Agilent Technologies, Santa Clara, CA, USA) on the Agilent 2100

Bioanalyzer. Library preparation of three technical replicates per developmental time-point/embryo, was performed on an Illumina HiSeq 4000 (150bp paired-end reads), according to the Illumina TruSeq Stranded mRNA Library Prep Kit protocol (Illumina Inc., San Diego, CA, USA). RNA sequencing analysis, candidate gene expression evaluation and causal network analysis, were performed as outlined in Supplementary Materials and Methods.

Quantitative Real Time (qRT)-PCR

cDNA was prepared from hindgut samples of three embryos from each time-point (EW12, EW14 and EW16), and qRT-PCR was performed on each sample using technical triplicates, as described before.¹⁶ Expression levels were normalized with two housekeeping genes (ACTB and GAPDH), and averaged. Primers used are described in Supplementary Table 4.

Statistical analysis

Data are expressed as mean \pm standard error of the mean. Differences in the data were evaluated between groups using one-way ANOVA and intergroup differences were determined by Tukey test or unpaired Student's t-test. P values < 0.05 were taken as statistically significant. The 'n values' reported refer to the number of individual fetal colonic segments used for each protocol.

Results

Development and maturation of key ENS cell types

To assess the development and maturation of the human fetal ENS, immunohistochemistry was performed on proximal colonic cryosections between EW12-16. This approach and time frame allowed for fate mapping of typical ENS cell types, including enteric neurons and glia within the second trimester. Human fetal colonic samples at EW12 displayed robust neuron specific TuJ1 expression, highlighting the presence of enteric neurons. The TuJ1⁺ cells, termed neurons from here on, were located within multiple discrete ganglia-like structures at the level of the myenteric plexus (**Fig. 1a&d, arrows**). Few TuJ1⁺ neurons were identified within the submucosal layer at EW12 (**Fig. 1a&d, arrowheads**). At this stage, SM22 staining, a marker of mature smooth muscle, revealed two distinct muscle layers (**Fig. 1a&d**), the inner circular layer (**Fig. 1d, asterix**) and outer longitudinal layer (**Fig. 1d, hash**), reflective of the morphology of the mature human enteric neuromusculature. Further maturation of the *tunica muscularis* was observed with thickening of muscle layers at EW14 (**Fig. 1b&e**) and EW16 (**Fig. 1c&f**). Notably, maturation and thickening of the circular muscle is more apparent across this time frame with SM22⁺ smooth muscle cells adopting a more uniform phenotype, with elongated nuclei in the circumferential orientation (**Fig. 1e&f, asterix**). Maturation of the ENS was also observed by EW14, as TuJ1⁺ ganglia within the myenteric plexus gradually coalesce and increase in size by EW14 (**Fig. 1b&e, arrows**). Interestingly, at this stage, more robust TuJ1⁺ expression was identified within the submucosal layer forming a rudimentary and interrupted submucosal plexus (**Fig. 1b&e, arrowheads**), with neuronal projections extending into mucosal villi. At EW16, TuJ1⁺ expression and localization were still observed in the myenteric plexus with further restriction of

ganglia-like structures (**Fig. 1c&f, arrows**). Further development of TuJ1⁺ neurons in the submucosal regions revealed a more continuous submucosal plexus (**Fig. 1c&f, arrowheads**) and TuJ1⁺ neuronal projections were also observed extending into mucosal villi.

To assess the development of enteric glial cells, expression of S100 was examined with immunohistochemistry over a similar time-frame. At EW12, S100 expression was observed within the myenteric plexus alongside robust TuJ1 expression (**Fig. 2a,d&g, arrows**). Such S100 expression appeared in isolation at this stage, with little co-expression of TuJ1 in either the myenteric plexus or submucosal layer (**Fig. 2a,d&g, arrows**). At EW14, occasional and weak co-expression of S100 and TuJ1 was observed in some cells both within the myenteric ganglia (**Fig. 2b,e&h, arrows**) and within the submucosal layer (**Fig. 2b,e&h, arrowheads**). Interestingly, weak S100 expression was additionally observed as a diffuse single cell layer on the serosal surface of EW14 tissue (**Fig. 2b,e&h, hash**). However, by EW16, this diffuse serosal S100 expression was no longer evident, and both S100⁺ glia (**Fig. 2c,f&i, arrowheads**) and TuJ1⁺ neurons (**Fig. 2c,f&i, arrows**) were observed discretely in close apposition within myenteric ganglia and in the submucosal plexus with little co-expression.

Neuronal subtype development in the human ENS

Having demonstrated the development of enteric neurons and glia as well as the maturation of ganglia from EW12-16, we further assessed the development of specific neuronal subtypes within the human fetal colon. Immunohistochemistry of proximal colonic sections at EW12 revealed co-expression of TuJ1 and vesicular acetylcholine transporter (VACht) (**Fig. 3a, Supplementary Fig.1a, arrows**) and substance P (Sub

P), within ganglia-like structures in the myenteric plexus (**Fig. 3d, Supplementary Fig.2a, arrows**). Robust VACHT⁺ expression was observed within myenteric ganglia (**Fig. 3b&c, Supplementary Fig.1b&c arrows**) and in the submucosal region (**Fig. 3b&c, arrowheads**) at both EW14 and EW16 respectively. Sub P was also observed to be more robustly expressed within myenteric ganglia (**Fig. 3e&f, Supplementary Fig.2b&c arrows**) and in the submucosal region at EW14 and EW16 (**Fig. 3e&f, arrowheads**). Interestingly, examination of inhibitory neuronal subtypes revealed no neuronal nitric oxide (nNOS; **Fig. 3g, Supplementary Fig.3a**) or vasoactive intestinal peptide (VIP; **Fig. 3j, Supplementary Fig.4a**) expression in EW12 colonic sections, despite robust TuJ1⁺ expression within the myenteric plexus. By EW14, TuJ1⁺ neurons were visualized both within the submucosal region and extending into mucosal villi (**Fig. 3h, arrowheads**), but the nNOS⁺ neurons were largely restricted to the myenteric plexus (**Fig. 3h, Supplementary Fig.3b arrows**) at this stage. Similarly, VIP co-labelled TuJ1⁺ neurons at the level of the myenteric plexus at EW14 (**Fig. 3k, Supplementary Fig.4b arrows**). However, VIP⁺ neurons were also visualized within the submucosal region at this stage, and extended processes into mucosal villi. With further development to EW16, more extensive nNOS⁺ (**Fig. 3i, Supplementary Fig.3c, arrows**) and VIP⁺ (**Fig. 3l, Supplementary Fig.4c, arrows**) expression was observed at the level of the myenteric plexus. Interestingly, nNOS⁺ neurons at EW16 appeared to remain restricted to the myenteric region with little co-expression in TuJ1⁺ neurons throughout the remaining gut wall (**Fig. 3i, arrowheads**). By contrast, strong VIP⁺ expression was observed in the submucosal region and within villus structures at EW16 (**Fig. 3l, arrowheads**). Taken together these data suggest that the initial development of excitatory neurons (VACHT and Sub

P) within the human fetal colon, occurs prior to EW12 whereas the development of inhibitory neurons (nNOS and VIP) occurs later, between EW12 and EW14.

Having demonstrated the maturation of the fetal ENS using cryosections, including the birth-dating of neuronal subtypes, we further assessed neural development in wholemount colonic preparations. Similar to cryosections, immunohistochemistry of EW12 wholemount colonic preparations revealed robust TuJ1⁺ neural networks at the level of the myenteric plexus. Here, TuJ1⁺ neurons were observed in complex anastomosing networks with ganglia like structures (**Fig. 4a, arrows**) and interganglionic neuronal connections (**Fig. 4b, arrowheads**). At EW14 (**Fig. 4b**) and EW16 (**Fig. 4c**), TuJ1⁺ immunohistochemistry revealed further network maturation including the development of dense neural connections (**Fig. 4b&c, arrows**), and formation of discrete ganglion structures (**Fig. 4b&c, arrowheads**).

Development of coordinated electrical activity in the human ENS

To assess the development of coordinated electrical activity within fetal tissues, calcium imaging of wholemount colonic preparations was performed from EW12-EW16. Little basal activity was observed in the presumptive ENS of EW12, EW14 or EW16 colonic preparations. However, occasional calcium transients in underlying smooth muscle cells were observed in basal conditions (**Supplementary Movies 1-3**). Upon electrical point stimulation, no stimulation-induced calcium transients were observed within (3/3) EW12 colonic samples ($\Delta F/F_0 = 1.033 \pm 0.002$; $n=3$, **Fig. 4d,g,j,m** & **Supplementary Movie 1**). Similarly, electrical stimulation did not elicit calcium transients within fetal tissues in the majority (4/5) of EW14 preparations ($\Delta F/F_0 = 1.055 \pm 0.029$; $n=5$; $P=0.813$ by Tukey test; **Fig. 4e,h,k,m** & **Supplementary Movie 2**). By EW16, there were statistically significant differences

in mean values of stimulation-induced calcium transients between control EW12, EW14 and EW16 groups, as determined by one-way analysis of variance (ANOVA) ($F(2,8)=11.36$, $P=0.0046$), with (3/3) EW16 colonic preparations displaying compound activation of the ENS (1.211 ± 0.026 ; $n=3$; **Fig. 4f,i,l,m&n**; **Supplementary Movie 3**) compared to either EW12 ($P=0.007$, Tukey test) or EW14 ($P=0.008$, Tukey test). Additionally, this stimulation-induced activation of enteric neuronal networks at EW16, was found to be blocked (3/3) in the presence of $1\mu\text{M}$ tetrodotoxin (1.029 ± 0.012 ; $n=3$), compared to stimulation in control conditions (1.211 ± 0.026 ; $n=3$; $P=0.0028$, Student's t-test; **Fig. 4o**; **Supplementary Movie 4**). This result suggests the presence of voltage-dependent sodium channels within the ENS at EW16 of human development.

To determine if the stimulation-induced compound activation observed at this stage could be due to the development of synaptic connectivity, we performed immunohistochemistry for synaptophysin across each of the time points examined. At EW12, co-expression of TuJ1 and synaptophysin was observed (**Fig. 5a, arrows**) within ganglia-like structures of the myenteric plexus. This co-expression was maintained at both EW14 and EW16 (**Fig. 5b&c, arrows**), with additional co-expression visualized within the submucosal region (**Fig. 5b&c, arrowheads**). These results suggest that while synaptic protein expression is in place by EW12, the development of stimulation-induced coordinated electrical activity is not established until later in development, between EW14 and EW16. To investigate if postsynaptic specialization is a limiting factor in the development of compound activation within the developing ENS, pharmacological activation and blockade of nicotinic neurotransmission was performed at EW14 and EW16, respectively. At EW14 application of $1\mu\text{M}$ acetylcholine (ACh) led to significant contraction of fetal colonic

tissue. Interestingly, this application did not result in compound activation of the presumptive ENS (**Fig. 5d,e&h; Supplementary Movie 5**). By contrast, application of high K^+ (300mM) led to stimulation of robust calcium transients within the presumptive ENS, and contraction of the tissue (**Fig. 5f,g&h; Supplementary Movie 5, n=2**). Furthermore, by EW16 when electrical stimulation was found to elicit calcium transients within the ENS (**Fig. 5i,j&o; Supplementary Movie 6**), application of 300 μ M hexamethonium (Hex) did not diminish such responses (**Fig. 5k,l&o; Supplementary Movie 6, n=1**) whereas, subsequent application of TTX (1 μ M) blocked compound activation of the fetal ENS (**Fig. 5m,n&o; Supplementary Movie 6**). Taken together these results suggest that both synaptic and postsynaptic specialization are not rate limiting factors in the development of stimulation-induced calcium activity in the early fetal ENS.

Transcriptional changes in the human fetal gut

To determine whether transcriptional changes might account for the apparent onset of electrical activity between EW14-16, RNA sequencing analysis was performed across all developmental stages (EW12, EW14 and EW16), using stringent and more lenient read alignment procedures. Only minor differences between these procedures were observed (see Supplementary Data Files *2-Lenient alignment* & *3-Stringent alignment*), allowing us to discriminate expression of different candidate gene homologues. Using either one of these alignments, 13,828 genes were found to be expressed during EW12-EW16. Very low transcript levels were detected for 8,612 genes, making interpretation difficult, since such low levels may represent noise. For 30,828 genes, we were unable to detect any transcripts. Using stage specific analysis parameters (CPM > 2 in specific EW week and <1 in the remaining two), few of the

detected genes were found to be specific for each of the time points included in this study (43 in EW12, 70 in EW14 and 80 in EW16). Many genes were also found to have different expression levels between EW12 and EW14 (n=2265), EW14 and EW16 (n=3610) and between EW12 and EW16 (n=3792). Most of these genes are known to affect many canonical pathways and biological functions, more than expected by chance alone. Comparing EW12 to EW14 and EW16, we could see that from a neuronal perspective, interesting characteristics and biological functions such as axogenesis, neuronal and synaptic development, quantity of neurons and neuronal tissue, sprouting and ion transport were significantly enriched (negative Z-score). Moreover, we observed that expression of mRNA encoding proteins that may contribute to functions such as Ca^{2+} flux, cation, divalent cation, ionic and Ca^{2+} mobilization, were significantly up-regulated (negative Z-score) when compared to earlier time-points (EW12 to EW14), but were downregulated (positive Z score) at later stages (EW14 to EW16; see Supplementary Data File 1-*Pathway enrichment*). To validate these results, we specifically looked at the expression levels of 36 genes known to encode ion channels, neuronal subtypes, glial cells, synapsins and semaphorins. We initially analysed expression by plotting their CPM values in a heat-plot (**Fig. 6 and Supplementary Fig. 5**). This approach revealed upregulation of almost all of these genes in EW14 and EW16 colonic tissue when compared to EW12. We also performed quantitative real time (qRT)-PCR analysis on three independent colonic samples from each developmental stage (EW12-16). The results obtained showed an upregulation of the expression levels of candidate Na^+ (SCN) and K^+ (KNCQ) channel expressing genes known to be involved in the generation and modulation of ENS action potentials. Each candidate ion channel examined (SCN2A, SCN3A, SCN5A, SCN8A, SCN9A, KCNQ2 and KCNQ3) displayed a trend towards

increased expression between EW12 and EW16 (**Fig. 7a, & Supplementary Table 1**). Notably, *SCN3A*, which encodes a TTX-sensitive fast inactivating voltage-gated Na^+ channel and plays a major role in neuronal action potentials, displayed a linear increasing trend in expression with a 1.10 fold increase at EW14 and 1.44 fold increase at EW16, compared to EW12 colonic tissue. Similarly, *SCN9A*, which has been shown to modify neuron excitability during the relative refractory period, displayed a linear increasing trend in expression with a 1.51 fold increase at EW14 and 2.13 fold increase at EW16, compared to EW12 colonic tissue. In contrast, other candidate genes, *KCNQ2* and *KCNQ3*, which encode delayed rectifier K^+ channels and act to regulate membrane excitability and the threshold for action potential generation, displayed increases in expression between EW12 and EW14, with subsequent reduction in expression at EW16. Upregulation of these ion channels might account for evoked activity at EW16. Concerning the expression levels of several ENS candidate genes, the expression patterns observed in terms of neuronal subtypes corresponded to the temporal development pattern observed in immunohistochemical analysis. *VACHT* expression was maintained at a relative constant level across the three developmental time-points (**Fig. 7b & Supplementary Table 1**), whereas nNOS expression displayed an increase at EW14, which corresponds to the birth-dating of this neuronal subtype. Expression of both *TAC-1*, a precursor of Sub P, and *VIP* also mimicked immunohistochemical observations, with increasing expression up to EW16. *S100* expression increased at EW14, which appears to match a possible transitional and transient period of S100^+ glial cell development, as visualized by immunofluorescence. Interestingly, *SYN1* expression remained relatively constant across each time point, supporting our earlier findings that synaptic proteins are already expressed by EW12. Finally, *SEMA3A*, a gut

morphogen previously found to affect ENS development, showed a modest increase in expression between EW12 and EW14, which appeared to plateau at EW16. Taken together these data suggest that rather than a significant shift in expression of a single ion channel or ion channel family, a trend in increasing expression of a range of critical ion channels appears to account for the changes in ENS neurotransmission across this four-week period. These data also confirm our immunohistochemical findings, further supporting the idea that the developmental time window between EW12-EW16 is critical for the establishment of a repertoire of neuronal subtypes and enteric glia.

Discussion

Extensive murine studies using immunohistochemical analysis and various reporter mice have established the temporal development pattern of the enteric nervous system (ENS), including the onset of spontaneous and induced electrical activity within embryonic mouse gut.^{4, 8-11, 17-25} However, such knowledge in the developing human gut is lacking. In this study, we report that the onset of evoked electrical activity within the human fetal ENS appears at approximately EW16. We demonstrate that such activity appears to coincide with increases in gene expression of various ion channels known to modulate enteric action potentials, and clearly establish the temporal development of a number of neural subtypes and enteric glia between EW12-EW16. Furthermore, we confirm such temporal development with gene expression studies that highlight the developmental processes required for the establishment of a functional ENS.

In this study the proximal colon was chosen as a site of investigation for both technical and translational purposes. The identification of the caecum in intestinal

specimens, across developmental timepoints, critically allowed for characterization of an anatomically consistent region (proximal colon) in all specimens. Moreover, the commonest congenital gut motility defects, including Hirschsprung disease and slow transit constipation, are known to affect the colonic region.²⁶ Therefore, a better understanding of the normal ENS developmental timeline, in this region, may provide a means of understanding factors and disease processes that influence functional development.

The formation of circuitry and the development of coordinated electrical activity are crucial requirements for 'normal' bowel function. Disruptions in neuronal plexus formation, density or diversity, severely impact physiological output.^{19, 27-31} In demonstrating the development of several key enteric neuronal subtypes from EW12-EW14, and the subsequent development of coordinated electrical activity at EW16, we believe that this four week developmental time period is critical for the 'correct' assembly of a functional ENS. Of note, the current study examined the development of evoked activity in the proximal colon and as such, the findings presented may not be reflective of the functional development of other gut segments. Importantly, recent studies in animal models have highlighted that routinely available pharmacological agents such as ibuprofen or vitamin A deficiency can impact ENS development.^{32, 33} Hence, it is conceivable that in this critical developmental window within the early second trimester, the ENS is vulnerable to insult which may be clinically relevant in terms of subtle disease processes.

Interestingly, our findings from both RNAseq and qRT-PCR analyses suggest a general upregulation of a number of ion channels and increasing diversity of enteric neurons and glia over this period. It should be noted that the methodology used in the current study utilised whole tissue segments rather than direct isolation of native

ENCC. As such, the inclusion of non-ENCC may have diluted the expression of specific ENCC related genes and may account for the failure of our comparison analysis to reach statistical significance. A previous murine study has demonstrated a similar general upregulation of ion channel expression between E11.5 and E14.5.³⁴ This study made use of endogenous YFP expression in murine ENCC to enable specific isolation of ENCC at each time-point, via fluorescence activated cell sorting (FACS). Whilst previous studies have successfully isolated small numbers of ENCC from human fetal tissue^{15,35} using p75 FACS isolation, the limited availability of fetal human gut samples and the need for physiological and immunohistochemical analyses in the current study, prevented the specific isolation of sufficient numbers of ENCC. Furthermore, one embryo per time-point was examined for this initial analysis, and the “groups” presented in the differential expression analysis represent technical replicates. Therefore, our differential expression analysis should be viewed as an indicator of the transcriptional difference between the developmental stages examined.

In this study, we clearly demonstrate that coordinated compound activation of enteric networks occurs between EW14 and EW16, revealing a critical period of gut development that may underpin functionality in later life. The finding that 4/5 human colon samples at EW14, did not display electrical activity compared with 3/3 at EW16 which did display Ca^{2+} transients upon electrical stimulation, suggests that this ‘window’ of activation is consistent across numerous fetal gut specimens. Similarly, immunohistochemical analysis of the temporal development of neural subtypes and glia was found to be consistent across multiple specimens. The staging method used in this study relies on measurement of either knee-to-heel length or foot length. While this method has been validated, the resolution of gestational age in weeks may lead to

minor discrepancies in precise staging. It is therefore likely that the sample (1/5) which displayed electrical activity at EW14 in response to stimulation, may represent late stage EW14/EW15 tissue. Interestingly, spontaneous Ca^{2+} oscillations were not resolved in the human ENS specimens examined. Previous investigations in murine gut samples suggest that spontaneous calcium transients occur from E11.5-E15.5, which can propagate to neighbouring ENCC. This spontaneous calcium activity appeared to be a transient phenomenon, as such activity was not observed in either E10.5 or E16.5 tissue.¹⁰ Given that this transient activity in mice commences prior to full colonization of the gut and then ceases shortly after ENCC have completed their rostrocaudal migration along the length of the gut, it is likely that spontaneous calcium activity was not observed in human specimens due to the time-frame of our current study, as complete colonization of the human gut has been shown to occur by approximately EW7.

The finding that inhibitory neuronal subtypes in the colon, including nNOS and VIP, appear to arise at approximately EW14 after excitatory neuronal subtypes (VACHT and Sub P), suggests that there is an extended period of neuronal modulation after ENCC colonization. Notably, in murine studies ChAT⁺ neurons were found to develop within the colon from E14.5,¹⁰ whereas nNOS⁺ neurons have previously been shown to arise between E12.5⁸ and E13.5 (E11.5 + 48-hour culture).¹⁸ The reasons behind the contrasting findings in terms of neuronal birth-dating are unclear. Unfortunately, in our hands, various immunohistological assays using ChAT antibodies in human gut tissue proved unsuccessful. However, complexities in the transcriptional and post-transcriptional regulation of ChAT and VACHT may account for the different timings observed in the two species.³⁶ Our finding that synaptic proteins are expressed at EW12, several weeks before the onset of coordinated

activity, suggests that while physical expression of synaptic proteins exist within the human ENS by the end of the first trimester, further modulation and refinement of the mechanisms involved in neuronal excitability occurs in the following weeks to allow coordinated, networked activity by EW16. Interestingly, we show that acetylcholine stimulation, at EW14, did not elicit compound activation of the presumptive ENS, and that blockade of nicotinic acetylcholine receptors at EW16 did not block stimulation-induced Ca^{2+} transients in the fetal ENS. Thus, this suggests that both synaptic and postsynaptic nicotinic specializations are not critical factors in the development of evoked calcium activity in the early human ENS.

Previous studies have suggested that neural activity may act to influence ENS wiring.^{17, 18} During mouse development, neurons transition from inactive to action potential (AP) firing with increasing voltage-gated sodium channel expression and increasing Na^+ current density.¹⁷ All embryonic action potentials in murine neurons in this study appeared to be TTX-sensitive. Similarly, in our current study, coordinated firing of enteric neural networks upon stimulation at EW16, were TTX-sensitive. Taken together, this suggests that a similar developmental pattern may be responsible for AP firing in early human fetal gut. The requirement for coordinated firing of the human ENS relatively early in gestation remains unclear. Whilst there is accumulation of meconium within the fetal human gut at early stages, fully developed motor patterns are not established until well into post-natal development.³⁷⁻³⁹ Therefore, further studies will be required to establish how the development of ENS activity in the human gut influences not only neural development *per se*, but the impact on associated cell types within the neuromuscular syncytium which ultimately dictate motility.

We conclude that this study provides critical evidence describing the birth-dating of neuronal subtypes and the subsequent emergence of coordinated electrical activity in the human ENS, and thus may provide a platform for future studies to understand the developmental and pathophysiological basis of enteric neuropathies in the human gastrointestinal tract.

ACCEPTED MANUSCRIPT

Figures Legends

Fig 1. Development and maturation of the enteric neuromusculature in the human fetal colon.

(**a-c**) Representative cryosection images at EW12 (a) EW14 (b) and EW16 (c) demonstrating the expression of TuJ1 (red), SM22 (green) and DAPI (blue). TuJ1⁺ neurons were identified within the myenteric plexus (arrows) and within the submucosal region (arrowheads). (**d-f**) High power images of EW12 (d) EW14 (e) and EW16 (f) demonstrating the expression of TuJ1 (red), SM22 (green) and DAPI (blue). TuJ1⁺ neurons were identified within the myenteric plexus (arrows) between the other longitudinal muscle (#) and inner circular muscle (*) layers together and within the submucosal region (arrowheads). Scale bars, 50µm

Fig 2. Development and maturation of the enteric glia in the human fetal colon.

(**a-f**) Representative cryosection images at low (a-c), medium (d-f) and high power (g-i) at EW12 (a,d,g) EW14 (b,e,h) and EW16 (c,f,i) demonstrating the expression of TuJ1 (red), S100 (green) and DAPI (blue). (**a,d,g**) At EW12, S100⁺ glial cells were identified within the myenteric plexus (arrows) in isolation, with little co-expression of TuJ1. (**b,e,h**) At EW14, occasional and weak co-expression of S100 and TuJ1 was observed within myenteric ganglia (arrows) and in the submucosal layer (arrowheads). Weak S100 expression was also observed as a diffuse layer on the serosal surface (#). (**c,f,i**) At EW16, discrete S100⁺ glia (arrowheads) and TuJ1⁺ neurons (arrows) were observed within myenteric ganglia and in the submucosal plexus. Scale bars, 50µm (a-f), 25µm (g-i).

Fig 3. Birth-dating of neuronal subtypes within the human fetal colon.

(a-c) Representative immunofluorescent images demonstrating expression of TuJ1 (red), VACht (green) and DAPI (blue). At EW12 (a) co-expression of TuJ1 and VACht was observed within the myenteric plexus (arrows) alone. At EW14 (b) and EW16 (c) co-expression was observed in the myenteric plexus (arrows) and in the submucosal region (arrowheads). **(d-f)** At EW12 (d) co-expression of TuJ1 and Sub P was observed within the myenteric plexus (arrows) alone. However, robust co-expression was observed in the myenteric plexus (arrows) and in the submucosal region (arrowheads) at EW14 (e) and EW16 (f). **(g-i)** At EW12 (g), expression of nNOS was not observed alongside TuJ1 in any region across the gut wall. At EW14 (h) co-expression of nNOS and TuJ1 was restricted to the myenteric plexus (arrows). TuJ1⁺ neurons were observed in the submucosal region extending into the villus crypts. These TuJ1⁺ neurons did not express nNOS. At EW16 (i) nNOS and TuJ1 co-expression was restricted in the myenteric plexus (arrows) with little nNOS co-expression in TuJ1⁺ neurons throughout the remaining gut wall (arrowheads). **(j-l)** TuJ1 expression was found in the myenteric plexus and sparsely in the submucosal region at EW12 (j) in the absence of VIP staining. At EW14 (k) co-expression of nNOS and TuJ1 was observed in the myenteric plexus (arrows) and the submucosal region and extending into the villus crypts (arrowheads). At EW16 (l) robust nNOS and TuJ1 co-expression was present in the myenteric plexus (arrows), the submucosal region, and extending into the villus crypts (arrowheads). Scale bars, 50µm

Fig 4. Induced calcium activity in the human fetal colon.

(a-c) Representative confocal z-stacks of wholemount colonic preparations. In EW12 (a), EW14 (b) and EW16 (c) wholemount colonic preparations showed robust TuJ1⁺ neural networks at the level of the myenteric plexus. Within the myenteric plexus TuJ1⁺ neurons were observed in complex anastomosing networks with ganglia-like structures (arrows) and interganglionic neuronal connections (arrowheads). **(d-f)** Wholemount preparations loaded with Fluo-4AM calcium indicator. **(g-i)** Representative pseudo-coloured images at t=0s in EW12 (g), EW14 (h) and EW16 (i). **(j-l)** Representative pseudo-coloured images at t=22s, after electrical stimulation, in EW12 (g), EW14 (h) and EW16 (i) preparations. Arrows represent regions of interest (ROI) shown in representative traces below. **(m)** Representative traces of calcium activity in ROI's indicated in (g-l), magenta arrow represents time of stimulation. Note the absence of any induced calcium transient in EW12 and EW14 colonic preparation. In contrast, calcium transients were observed upon stimulation in EW16 preparations. **(n)** Summary data showing peak stimulation-induced calcium activity ($\Delta F/F_0$) in EW12 (grey bar; n=3), EW14 (blue bar; n=5) and EW16 (red bar; n=3) colonic preparations. ** denotes $P < 0.01$ by Tukey test. **(o)** Summary data showing peak stimulation-induced calcium activity ($\Delta F/F_0$) in EW16 colonic preparations in control conditions (solid red bar; n=3) and after application of 1 μ M TTX (hashed red bar; n=3). ** denotes $P < 0.01$ by Student's t-test.

Fig 5. Synaptic protein expression and functional postsynaptic specialization in the human fetal colon.

(a-c) Representative high power immunofluorescent images of colonic cryosections at EW12 (a), EW14 (b) and EW16 (c) demonstrating the expression of TuJ1 (red), Synaptophysin (SYP, green) and DAPI (blue). (a) At EW12 co-expression of TuJ1 and synaptophysin was observed within ganglia-like structures of the myenteric plexus (arrows). **(b,c)** At EW14 and EW16 co-expression of TuJ1 and synaptophysin was observed within the myenteric plexus region (arrows) and within the submucosal region (arrowheads). Scale bars, 50 μ m. **(d-h)** Representative activity of EW14 fetal colonic tissue in the presence of acetylcholine (1 μ M) and high K⁺. **(d,e)** Pseudo-coloured images of calcium activity within the presumptive ENS at t=0s (d) and t=22s (e), after application of acetylcholine (1 μ M). **(f,g)** Pseudo-coloured images of calcium activity at t=0s (f) and t=22s (g), after application of high K⁺. Arrows represent regions of interest (ROI) shown in representative traces shown in h. **(h)** Representative traces of calcium activity in ROI's indicated in (d-g), magenta arrow represents time of pharmacological application. **(i-n)** Representative pseudo-coloured images of calcium activity within the ENS at t=0s and, after electrical stimulation, at t=27s in control conditions (krebs; i,j), in the presence of hexamethonium (300 μ M; k,l) and after the application of TTX (1 μ M; m,n). Arrows represent regions of interest (ROI) shown in representative traces shown in o. **(o)** Representative traces of calcium activity in ROI's indicated in (i-n), magenta arrow represents time of electrical stimulation.

Fig 6. Representative gene expression heat-plot for candidate genes in the human fetal colon.

Heat-plot based on RNA-seq analysis (lenient analysis parameters) (left) of individual fetal colon samples, showing gene expression (left) at EW12, EW14 and EW16 [low relative expression (red) and high relative expression (green)]. Average expression by time-point (right) shows directionality of expression from lower expression (red) to higher expression (green). Significant changes in gene expression represent FDR values ≤ 0.05 .

Fig 7. qRT-PCR analysis of candidate gene expression in the human fetal colon.

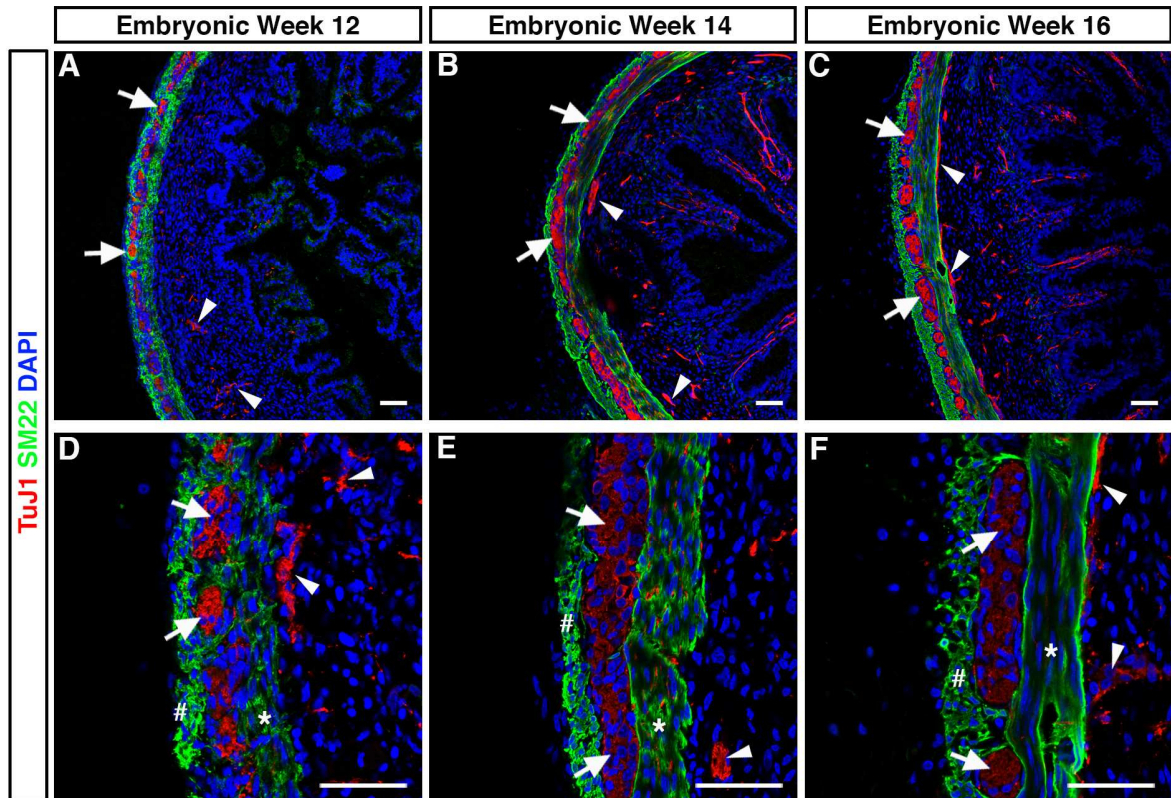
(a) Quantification of candidate ion channel gene expression in EW12 (grey bars), EW14 (blue bars) and EW16 (red bars). (b) Quantification of candidate gene expression for markers for enteric neurons and glia in EW12 (grey bars), EW14 (blue bars) and EW16 (red bars).

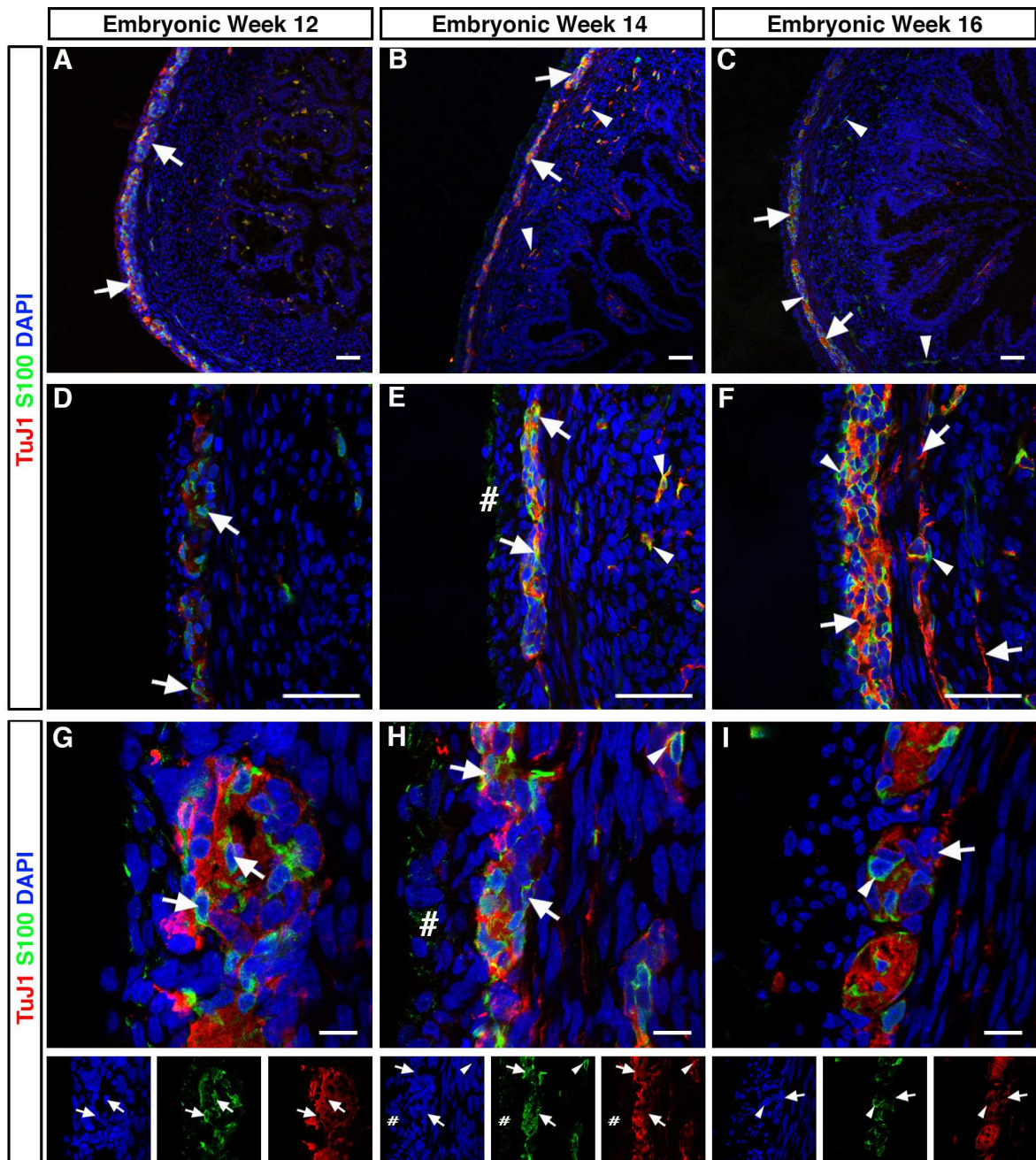
References

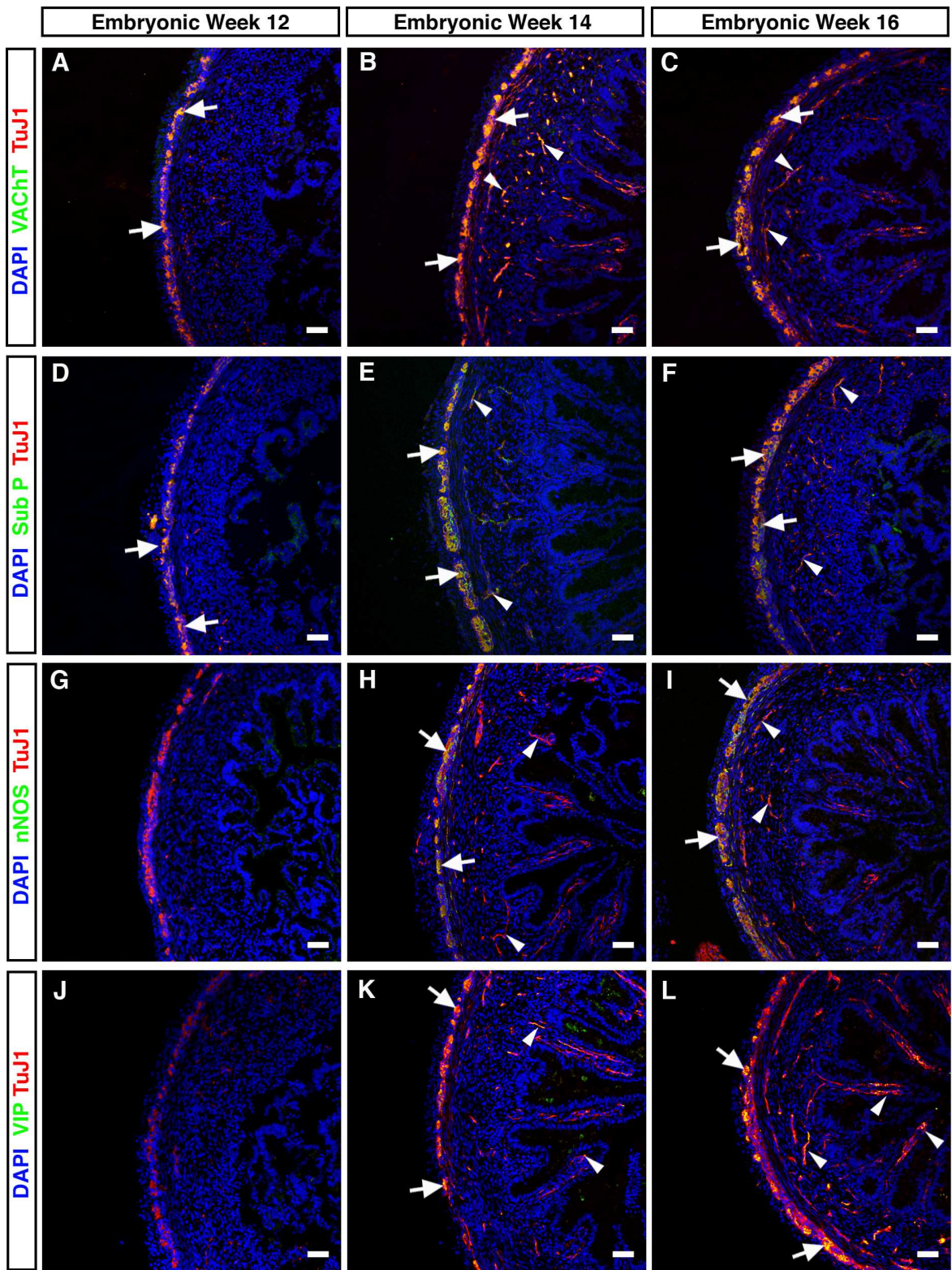
1. Furness JB. The enteric nervous system. Malden, Mass.: Blackwell Pub., 2006.
2. Burns AJ, Douarin NM. The sacral neural crest contributes neurons and glia to the post-umbilical gut: spatiotemporal analysis of the development of the enteric nervous system. *Development* 1998;125:4335-47.
3. Kapur RP, Yost C, Palmiter RD. A transgenic model for studying development of the enteric nervous system in normal and aganglionic mice. *Development* 1992;116:167-75.
4. Young HM, Hearn CJ, Ciampoli D, et al. A single rostrocaudal colonization of the rodent intestine by enteric neuron precursors is revealed by the expression of Phox2b, Ret, and p75 and by explants grown under the kidney capsule or in organ culture. *Dev Biol* 1998;202:67-84.
5. Wang X, Chan AK, Sham MH, et al. Analysis of the sacral neural crest cell contribution to the hindgut enteric nervous system in the mouse embryo. *Gastroenterology* 2011;141:992-1002 e1-6.
6. Nishiyama C, Uesaka T, Manabe T, et al. Trans-mesenteric neural crest cells are the principal source of the colonic enteric nervous system. *Nat Neurosci* 2012;15:1211-8.
7. Lasrado R, Boesmans W, Kleinjung J, et al. Lineage-dependent spatial and functional organization of the mammalian enteric nervous system. *Science* 2017;356:722-726.
8. Young HM, Jones BR, McKeown SJ. The projections of early enteric neurons are influenced by the direction of neural crest cell migration. *J Neurosci* 2002;22:6005-18.
9. Hao MM, Bornstein JC, Young HM. Development of myenteric cholinergic neurons in ChAT-Cre;R26R-YFP mice. *J Comp Neurol* 2013;521:3358-70.
10. Hao MM, Bergner AJ, Hirst CS, et al. Spontaneous calcium waves in the developing enteric nervous system. *Dev Biol* 2017;428:74-87.
11. Hao MM, Boesmans W, Van den Abbeel V, et al. Early emergence of neural activity in the developing mouse enteric nervous system. *J Neurosci* 2011;31:15352-61.
12. Fu M, Tam PK, Sham MH, et al. Embryonic development of the ganglion plexuses and the concentric layer structure of human gut: a topographical study. *Anat Embryol (Berl)* 2004;208:33-41.
13. Wallace AS, Burns AJ. Development of the enteric nervous system, smooth muscle and interstitial cells of Cajal in the human gastrointestinal tract. *Cell Tissue Res* 2005;319:367-82.
14. Cooper JE, McCann CJ, Natarajan D, et al. In Vivo Transplantation of Enteric Neural Crest Cells into Mouse Gut; Engraftment, Functional Integration and Long-Term Safety. *PLoS One* 2016;11:e0147989.
15. Cooper JE, Natarajan D, McCann CJ, et al. In vivo transplantation of fetal human gut-derived enteric neural crest cells. *Neurogastroenterol Motil* 2017;29:e12900.
16. Halim D, Wilson MP, Oliver D, et al. Loss of LMOD1 impairs smooth muscle cytocontractility and causes megacystis microcolon intestinal hypoperistalsis syndrome in humans and mice. *Proc Natl Acad Sci U S A* 2017;114:E2739-E2747.

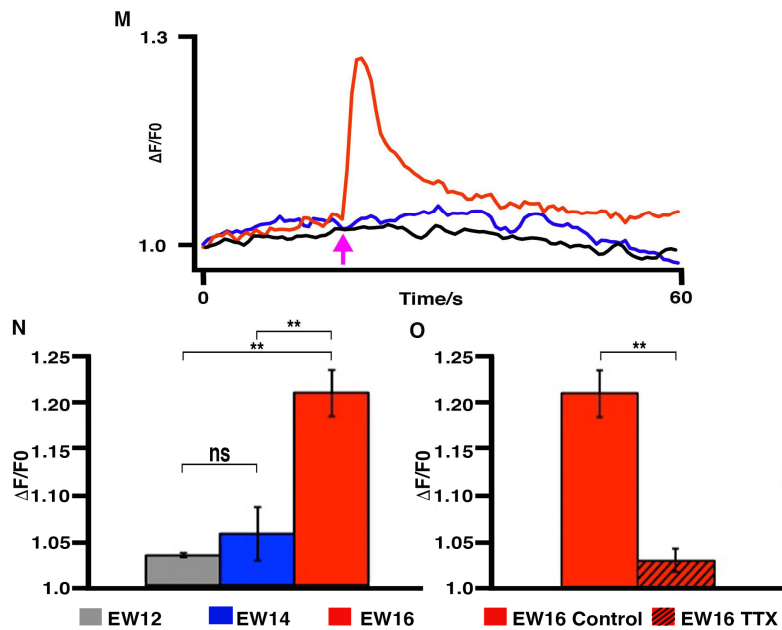
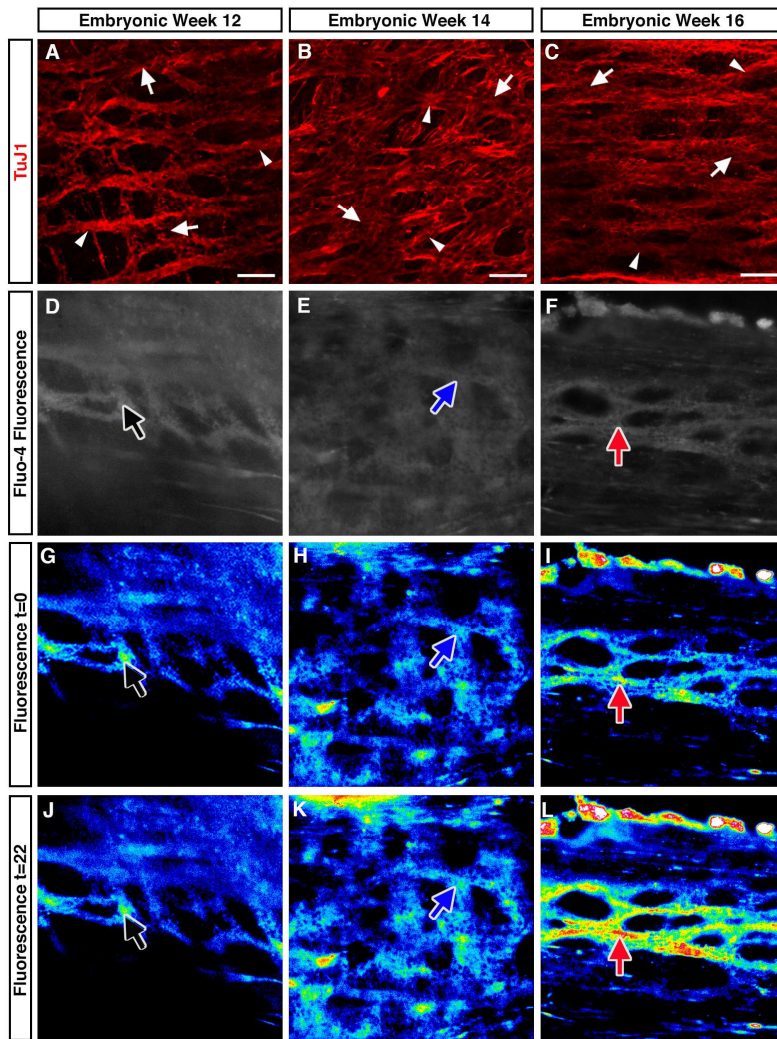
17. Hao MM, Lomax AE, McKeown SJ, et al. Early development of electrical excitability in the mouse enteric nervous system. *J Neurosci* 2012;32:10949-60.
18. Hao MM, Moore RE, Roberts RR, et al. The role of neural activity in the migration and differentiation of enteric neuron precursors. *Neurogastroenterol Motil* 2010;22:e127-37.
19. Sasselli V, Boesmans W, Vanden Berghe P, et al. Planar cell polarity genes control the connectivity of enteric neurons. *J Clin Invest* 2013;123:1763-72.
20. Young HM, Bergner AJ, Anderson RB, et al. Dynamics of neural crest-derived cell migration in the embryonic mouse gut. *Dev Biol* 2004;270:455-73.
21. Foong JP, Hirst CS, Hao MM, et al. Changes in Nicotinic Neurotransmission during Enteric Nervous System Development. *J Neurosci* 2015;35:7106-15.
22. Foong JP, Nguyen TV, Furness JB, et al. Myenteric neurons of the mouse small intestine undergo significant electrophysiological and morphological changes during postnatal development. *J Physiol* 2012;590:2375-90.
23. Foong JP, Tough IR, Cox HM, et al. Properties of cholinergic and non-cholinergic submucosal neurons along the mouse colon. *J Physiol* 2014;592:777-93.
24. Fung C, Boesmans W, Cirillo C, et al. VPAC Receptor Subtypes Tune Purinergic Neuron-to-Glia Communication in the Murine Submucosal Plexus. *Front Cell Neurosci* 2017;11:118.
25. Koussoulas K, Swaminathan M, Fung C, et al. Neurally Released GABA Acts via GABAC Receptors to Modulate Ca(2+) Transients Evoked by Trains of Synaptic Inputs, but Not Responses Evoked by Single Stimuli, in Myenteric Neurons of Mouse Ileum. *Front Physiol* 2018;9:97.
26. Pesce M, Borrelli O, Saliakellis E, et al. Gastrointestinal Neuropathies: New Insights and Emerging Therapies. *Gastroenterol Clin North Am* 2018;47:877-894.
27. Kapoor A, Auer DR, Lee D, et al. Testing the Ret and Sema3d genetic interaction in mouse enteric nervous system development. *Hum Mol Genet* 2017;26:1811-1820.
28. McCann CJ, Cooper JE, Natarajan D, et al. Transplantation of enteric nervous system stem cells rescues nitric oxide synthase deficient mouse colon. *Nat Commun* 2017;8:15937.
29. Uesaka T, Enomoto H. Neural precursor death is central to the pathogenesis of intestinal aganglionosis in Ret hypomorphic mice. *J Neurosci* 2010;30:5211-8.
30. Brun P, Giron MC, Qesari M, et al. Toll-like receptor 2 regulates intestinal inflammation by controlling integrity of the enteric nervous system. *Gastroenterology* 2013;145:1323-33.
31. Anitha M, Gondha C, Sutliff R, et al. GDNF rescues hyperglycemia-induced diabetic enteric neuropathy through activation of the PI3K/Akt pathway. *J Clin Invest* 2006;116:344-56.
32. Fu M, Sato Y, Lyons-Warren A, et al. Vitamin A facilitates enteric nervous system precursor migration by reducing Pten accumulation. *Development* 2010;137:631-40.
33. Schill EM, Lake JI, Tusheva OA, et al. Ibuprofen slows migration and inhibits bowel colonization by enteric nervous system precursors in zebrafish, chick and mouse. *Dev Biol* 2016;409:473-88.

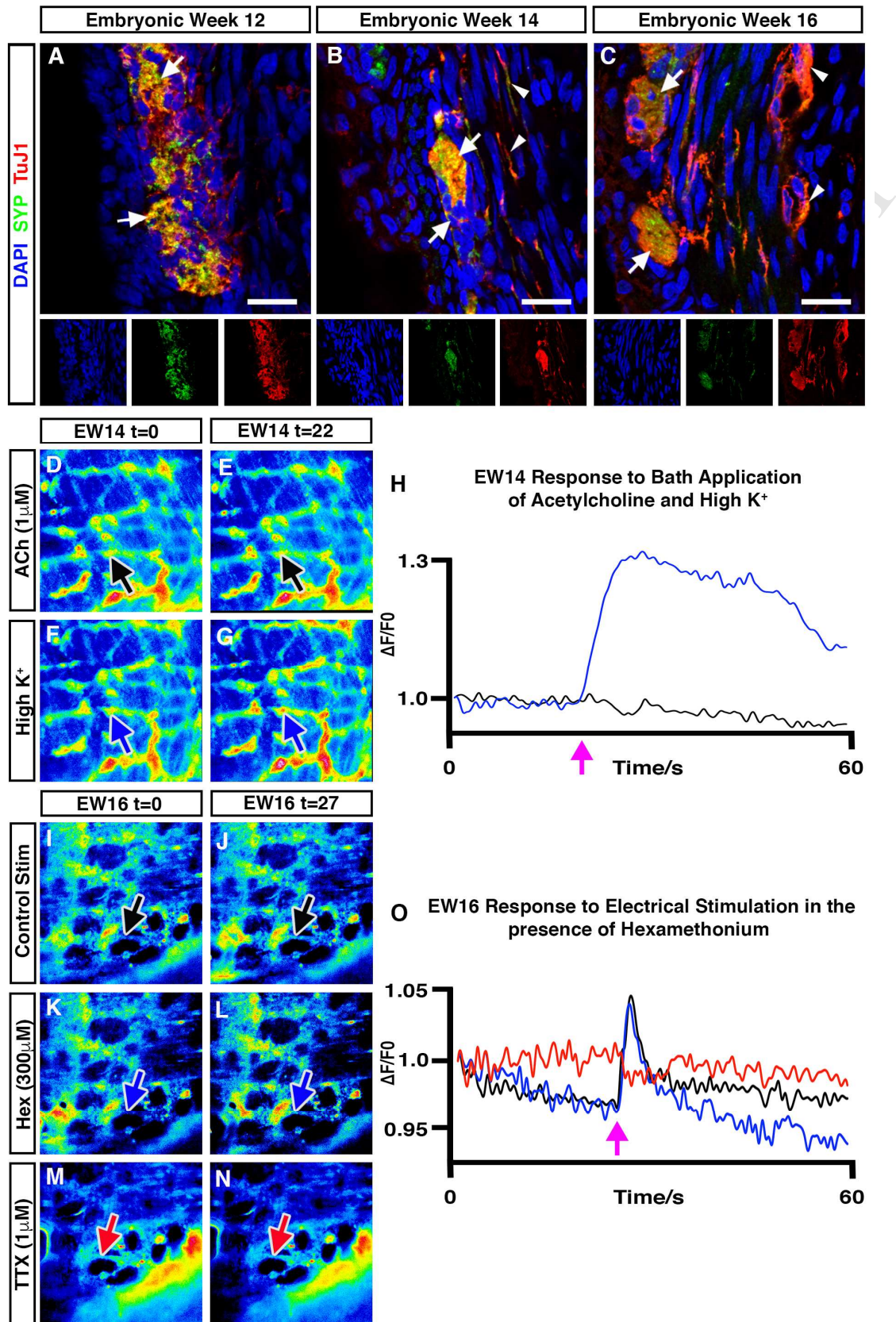
34. Hirst CS, Foong JP, Stamp LA, et al. Ion channel expression in the developing enteric nervous system. *PLoS One* 2015;10:e0123436.
35. Metzger M, Caldwell C, Barlow AJ, et al. Enteric nervous system stem cells derived from human gut mucosa for the treatment of aganglionic gut disorders. *Gastroenterology* 2009;136:2214-25
36. Castell X, Diebler MF, Tomasi M, et al. More than one way to toy with ChAT and VACht. *J Physiol Paris* 2002;96:61-72.
37. Bisset WM, Watt JB, Rivers RP, et al. Measurement of small-intestinal motor activity in the preterm infant. *J Biomed Eng* 1988;10:155-8.
38. Baker J, Berseth CL. Postnatal change in inhibitory regulation of intestinal motor activity in human and canine neonates. *Pediatr Res* 1995;38:133-9.
39. Amarnath RP, Berseth CL, Malagelada J-R, et al. Postnatal Maturation of Small Intestinal Motility in Preterm and Term Infants. *Neurogastroenterology & Motility* 1989;1:138-143.

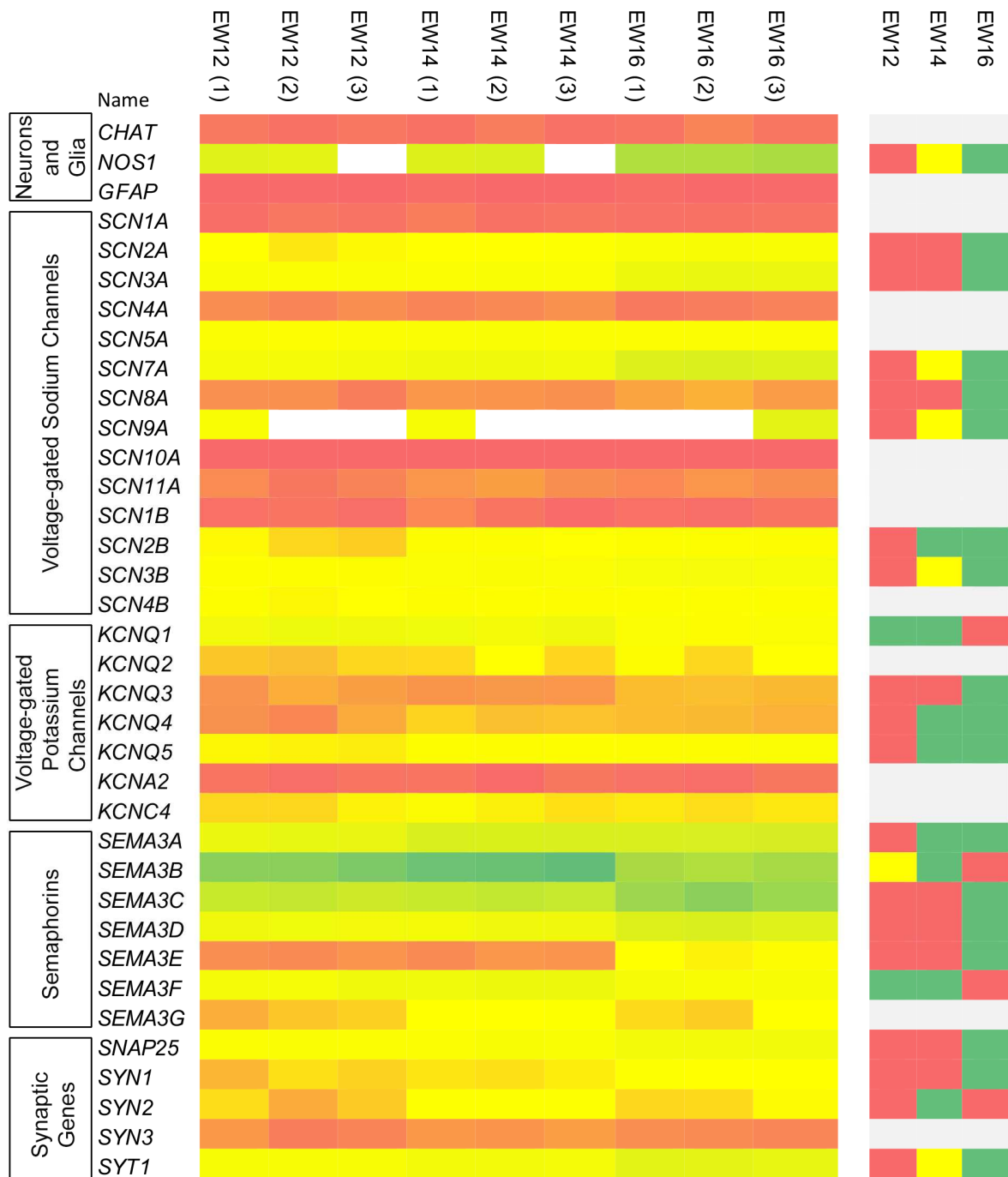


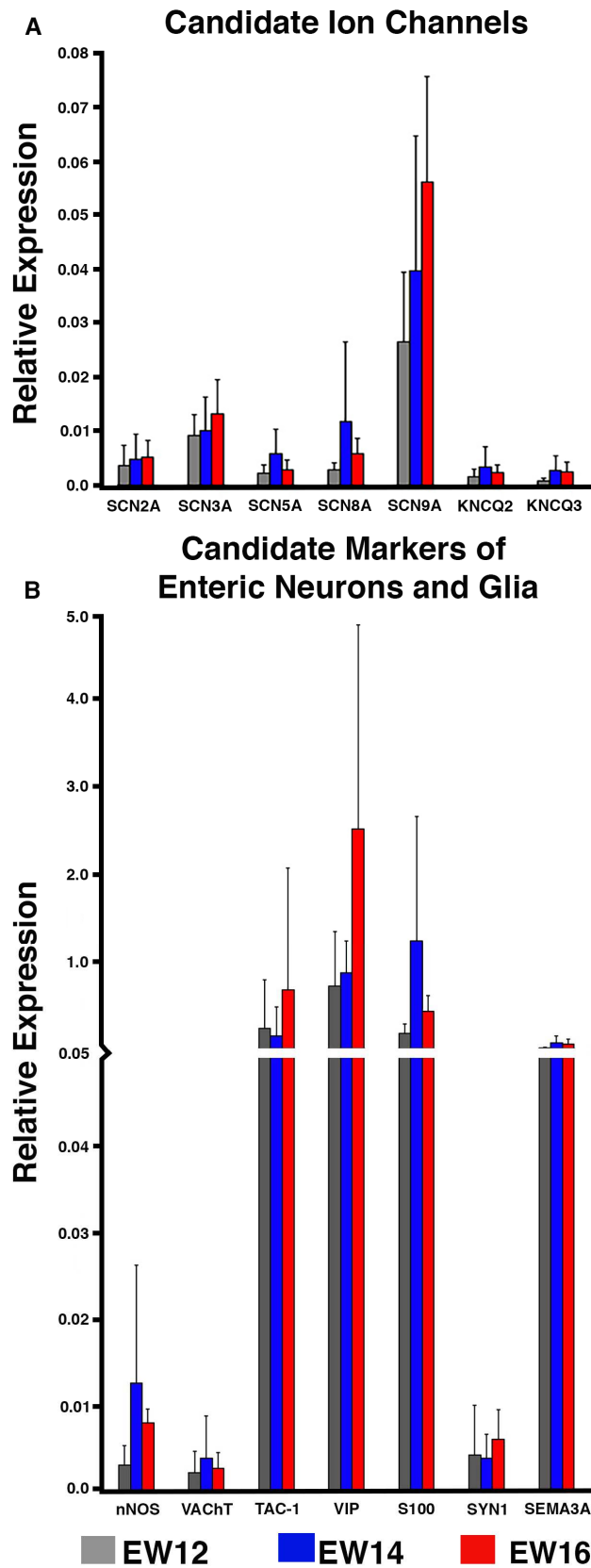






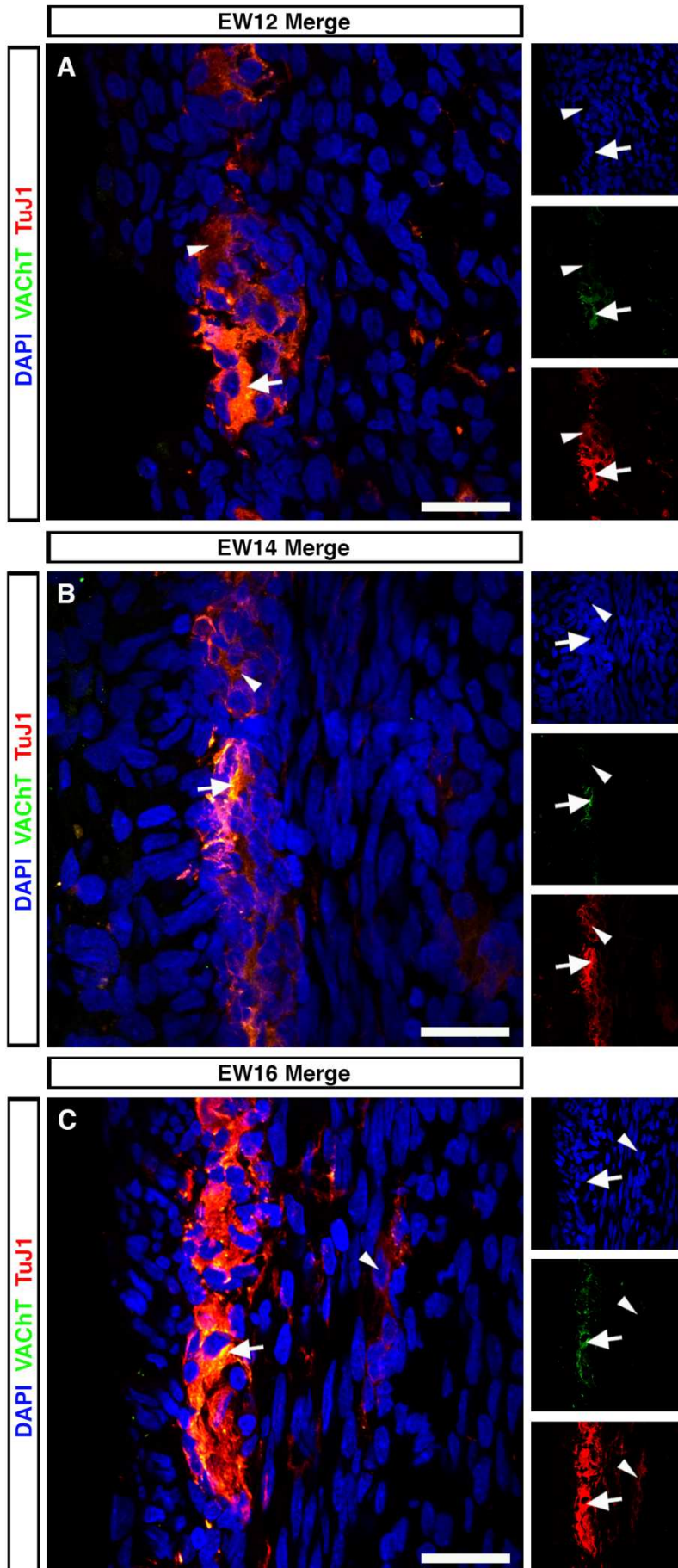






Supplementary Figures and Tables

ACCEPTED MANUSCRIPT

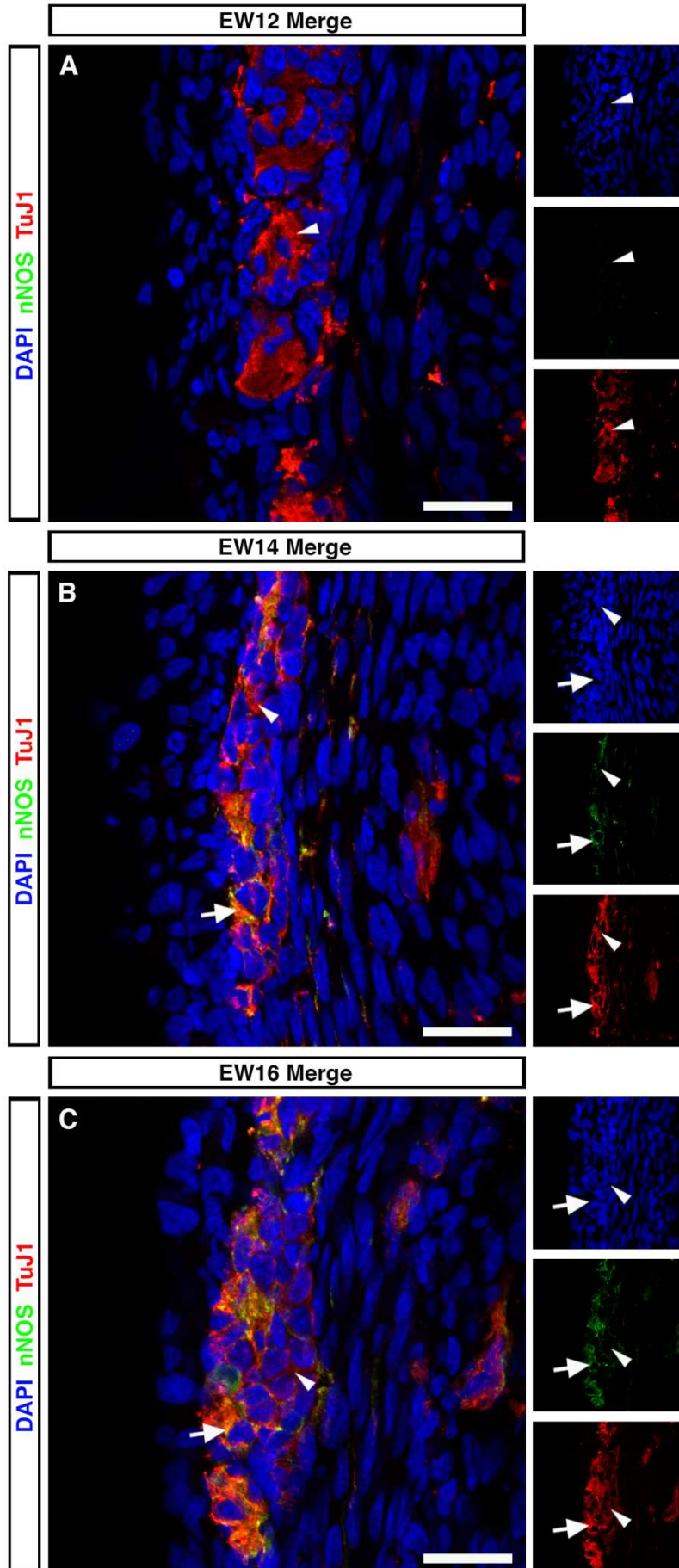


Supplementary Fig. 1. Development of VACHT⁺ neurons in the human fetal colon.

(a-c) Representative high-power immunofluorescent images demonstrating expression of TuJ1 (red), VACHT (green) and DAPI (blue) in the developing fetal colon. At EW12 (a), EW14 (b) and EW16 (c) co-expression of TuJ1 and VACHT was observed in numerous cells at the level of the myenteric plexus (arrows). In addition, TuJ1⁺ cells not expressing VACHT were observed (arrowheads). Scale bars, 25 μ m.

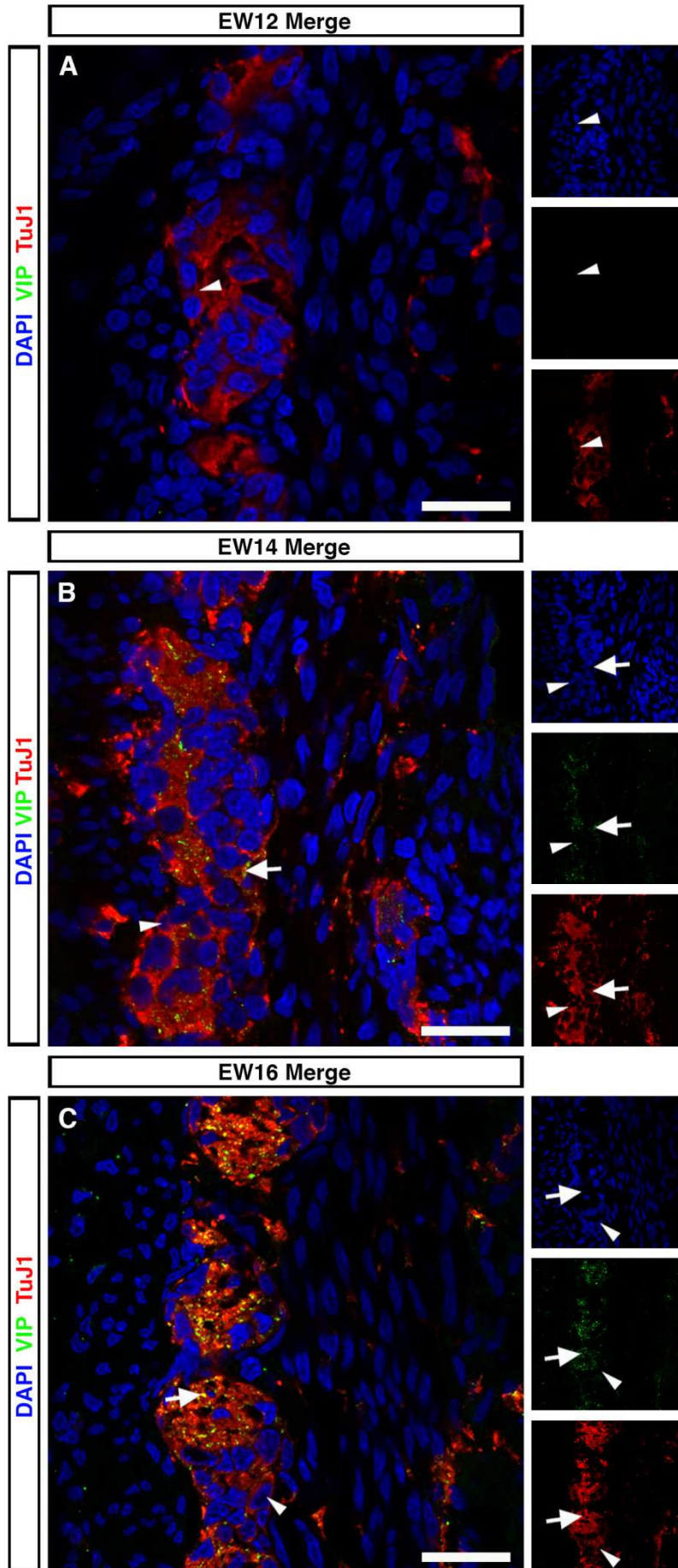
Supplementary Fig. 2. Development of Sub P⁺ neurons in the human fetal colon.

(a-c) Representative high-power immunofluorescent images demonstrating expression of TuJ1 (red), Sub P (green) and DAPI (blue) in the developing fetal colon. At EW12 (a), EW14 (b) and EW16 (c) co-expression of TuJ1 and SubP was observed in cells within ganglia-like structures at the level of the myenteric plexus (arrows). In addition, TuJ1⁺ cells not expressing Sub P were observed (arrowheads). Scale bars, 25µm.



Supplementary Fig. 3. Development of nNOS⁺ neurons in the human fetal colon.

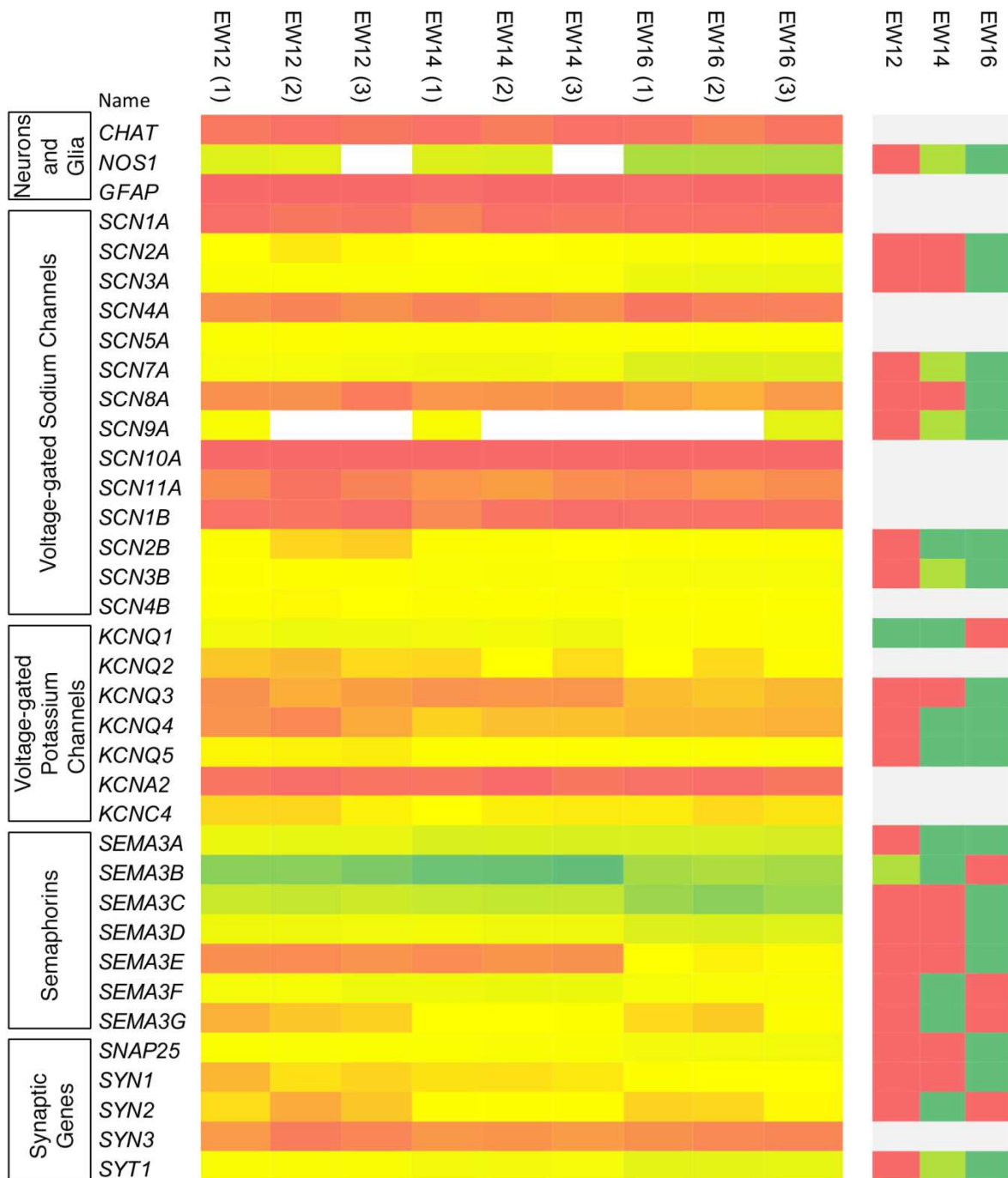
(a-c) Representative high-power immunofluorescent images demonstrating expression of TuJ1 (red), nNOS (green) and DAPI (blue) in the developing fetal colon. At EW12 (a), TuJ1 expression was observed alone with no evidence of nNOS expression. At EW14 (b) and EW16 (c) co-expression of TuJ1 and nNOS was observed in cells within-ganglia like structures at the level of the myenteric plexus (arrows). In addition, TuJ1⁺ cells not expressing nNOS were observed (arrowheads). Scale bars, 25 μ m.



Supplementary Fig. 4. Development of VIP⁺ neurons in the human fetal colon.

(a-c) Representative high-power immunofluorescent images demonstrating expression of TuJ1 (red), VIP (green) and DAPI (blue) in the developing fetal colon. At EW12 (a), TuJ1 expression was observed alone with no evidence of VIP expression. At EW14 (b) and EW16 (c) TuJ1⁺ cells, at the level of the myenteric plexus, were observed displaying punctate VIP expression (arrows). In addition, TuJ1⁺ cells not expressing VIP were observed (arrowheads).

Scale bars, 25µm.



Supplementary Fig. 5. Representative gene expression heat-plot for candidate genes in the human fetal colon.

Heat-plot based on RNA-seq analysis (stringent analysis parameters) of individual fetal colon samples, showing gene expression (left) at EW12, EW14 and EW16 [low relative expression (red) and high relative expression (green)]. Average expression by time-point (right) shows

directionality of expression from lower expression (red) to higher expression (green).

Significant changes in gene expression represent FDR values ≤ 0.05 .

ACCEPTED MANUSCRIPT

Supplementary Table 1.

Gene	Relative Expression \pm SD			P value
	EW12	EW14	EW16	
SCN2A	0.004 \pm 0.004	0.005 \pm 0.005	0.005 \pm 0.003	0.888
SCN3A	0.009 \pm 0.004	0.010 \pm 0.006	0.013 \pm 0.006	0.433
SCN5A	0.002 \pm 0.002	0.006 \pm 0.005	0.003 \pm 0.002	0.128
SCN8A	0.003 \pm 0.001	0.012 \pm 0.015	0.006 \pm 0.003	0.233
SCN9A	0.026 \pm 0.013	0.040 \pm 0.025	0.056 \pm 0.019	0.056
KCNQ2A	0.001 \pm 0.001	0.003 \pm 0.003	0.002 \pm 0.001	0.228
KCNQ3A	0.001 \pm 0.001	0.003 \pm 0.003	0.002 \pm 0.002	0.305
nNOS	0.003 \pm 0.002	0.013 \pm 0.013	0.008 \pm 0.002	0.112
VACHT	0.002 \pm 0.002	0.004 \pm 0.005	0.003 \pm 0.002	0.591
TAC-1	0.276 \pm 0.553	0.189 \pm 0.335	0.713 \pm 1.401	0.563
VIP	0.757 \pm 0.632	0.908 \pm 0.376	2.559 \pm 2.333	0.080
S100B	0.217 \pm 0.110	1.279 \pm 1.420	0.469 \pm 0.182	0.101
SYN1	0.004 \pm 0.006	0.004 \pm 0.003	0.006 \pm 0.003	0.649
SEMA3A	0.057 \pm 0.010	0.113 \pm 0.080	0.101 \pm 0.058	0.237

Supplementary Table 1. Analysis of candidate gene expression in the human fetal colon.

Comparison of the relative expression (mean Δ CT value \pm SD) of candidate genes in the human fetal colon at EW12, EW14 and EW16 as analysed by qRT-PCR. P values were calculated by Student's t-test

Supplementary Table 2. Primary Antibodies used for Immunohistochemistry

PRIMARY ANTIBODY	CONCENTRATION	COMPANY
Mouse anti-TuJ1	1:500	Biologend
Rabbit anti-TuJ1	1:500	Biologend
Rabbit anti-SM22	1:1000	Abcam
Mouse anti-S100	1:100	Abcam
Goat anti-VACHT	1:200	ThermoFisher Scientific
Rabbit anti-nNOS	1:400	Invitrogen
Mouse anti-Sub P	1:100	R&D Systems
Sheep anti-SNAP 25	1:200	R&D Systems
Mouse anti-Synaptophysin	1:250	Serotec

Supplementary Table 3. Secondary Antibodies used for Immunohistochemistry

SECONDARY ANTIBODY	ALEXA FLUOR	CONCENTRATION	COMPANY
Goat anti-mouse	488	1:500	Invitrogen
Goat anti-mouse	568	1:500	Invitrogen
Goat anti-rabbit	568	1:500	Invitrogen
Donkey anti-goat	488	1:500	Invitrogen
Donkey anti-sheep	488	1:500	Invitrogen
DAPI		1:1000	Sigma

Supplementary Table 4. Primers used for qRT-PCR

Gene	Primer (5'-3')
<i>SCN2AF</i>	TCCATGGAATTGGTTGGATT
<i>SCN2AR</i>	TTGTTTTCAATGCTCGGAGA
<i>SCN3AF</i>	TCCTCTGGAAGGCAAAGAG
<i>SCN3AR</i>	AACCATGCATCACAGCAGTC
<i>SCN5AF</i>	CTCACCAACTGCGTGTTTCAT
<i>SCN5AR</i>	CCTCGAGCCAGAATCTTGAC
<i>SCN8AF</i>	TGTGTGGCCATAAACTTCA
<i>SCN8AR</i>	GCATCAGAACTGTTCCCACA
<i>SCN9AF</i>	CCCAACCTCAGACAGAGAGC
<i>SCN9AR</i>	TGGAGAGCAATTCCAGATCA
<i>KCNQ2F</i>	TCGTGCTGTCTGTGTTTTCC
<i>KCNQ2R</i>	ATCCGCACGAAGTACTCCAC
<i>KCNQ3F</i>	ATTCTGGCTGTCCTGACCAC
<i>KCNQ3R</i>	ACTCGGCTCCAAAGATGAAA
<i>nNOSF</i>	ACAGTCCCCCACAAAGAATG
<i>nNOSR</i>	GGAGCCCATGCAGATGTACT
<i>SEMA3AF</i>	AAGGGATCAGCCGTGTGTAT
<i>SEMA3AR</i>	CCTTGATAAGGCACCCATTG
<i>SYNIF</i>	GCCAATGGTGGATTCTCTGT
<i>SYNIR</i>	AACTGCGGTAGTCTCCGTTG
<i>VIPF</i>	GCTCCTTGTGCTCCTGACTC
<i>VIPR</i>	GGTTCATTTGCTCCCTCAA
<i>TAC1F</i>	TGTTGGACTAATGGGCAAAA
<i>TAC1R</i>	TGTTGGACTAATGGGCAAAA
<i>VACHTF</i>	ACTATGCGGCCTCTGTTTTG
<i>VACHTR</i>	AATAGGAGATGTCGGCGATG
<i>S100BF</i>	ATTCTGGAAGGGAGGGAGAC
<i>S100BR</i>	TCCACAACCTCCTGCTCTTT
<i>ACTBF</i>	AACCGCGAGAAGATGACCC
<i>ACTBR</i>	GCCAGAGGCGTACAGGGATAG
<i>GAPDHf</i>	CGACCTTCACCTTCCCCAT
<i>GAPDHR</i>	TAAAAGCAGCCCTGGTGACC

Supplementary Materials and Methods

Immunohistochemistry

Wholemount immunohistochemistry was performed on fetal colonic segments after excision and removal of the mucosa by sharp dissection as. Tissues were fixed in paraformaldehyde (4% w/v in 0.1 mol L⁻¹ PBS for 45 min at 22°C), washed for 24 h in PBS (0.01 mol L⁻¹, pH 7.2 at 4°C), blocked for 1h (0.1 mol L⁻¹ PBS containing 1% Triton X-100, 1% BSA) and incubated in primary antibody (diluted in 0.1 mol L⁻¹ PBS containing 1% Triton X-100, 1% BSA, Supplementary Table 2) for 48h at 4°C. Immunoreactivity was detected using the secondary antibodies listed in Supplementary Table 3 (1:500 in 0.1 mol L⁻¹ PBS, 1 h at room temperature). Before mounting, tissues were washed thoroughly in PBS (0.1 mol L⁻¹ PBS for 2h at 22 °C).

For cryostat sections, colonic tissues were fixed in paraformaldehyde (4% w/v in 0.1 mol L⁻¹ PBS for 45 min at 22°C) after excision, washed for 24 h in PBS (0.01 mol L⁻¹, pH 7.2 at 4°C), cryoprotected in 0.1 mol L⁻¹ PBS containing 30% sucrose (24h at 4°C) and embedded in gelatin (7.5% w/v in 0.1 mol L⁻¹ PBS containing 15% sucrose). Subsequently tissues were frozen at -65°C in isopentane and stored at -80°C. Frozen, embedded samples were sectioned serially (20µm) using a Cam 1900 UV Cryostat (Leica Microsystems, UK) and slides stored at -20°C for further processing.

For cryosection immunohistochemistry, slides were thawed and heated to 37°C in 0.01 mol L⁻¹ PBS for 20 min to remove excess gelatin. Tissues were post-fixed in paraformaldehyde (4% w/v in 0.1 mol L⁻¹ PBS for 10 min at 22°C), washed 3 x 20 min in PBS (0.01 mol L⁻¹, pH 7.2 at 4°C), blocked for 1h (0.1 mol L⁻¹ PBS containing 1% Triton X-100, 1% BSA). Tissues were incubated in primary and secondary antibody as described above. Before mounting, sections were washed thoroughly in PBS (0.1 mol L⁻¹ PBS 3 x 20 min at 22 °C). Control tissues were prepared by omitting primary or secondary antibodies.

Tissues and sections were examined using a LSM710 Meta confocal microscope (Zeiss, Germany). Wholemout confocal micrographs were digital composites of the Z-series of scans (0.5 μ m optical sections) and confocal micrographs of cryostat sections were single plane images. Final images were constructed using FIJI software.³⁵

Calcium imaging

Fetal intestinal samples were obtained as previously described and calcium imaging was performed as previously published.²⁹ Briefly, tissues were immersed in previously oxygenated (95% oxygen/5% carbon dioxide) Krebs solution (in mM: 120.9 NaCl, 5.9 KCl, 1.2 MgCl₂, 2.5 CaCl₂, 11.5 glucose, 14.4 NaHCO₃ and 1.2 NaH₂PO₄). After excision of the colon and removal of the mucosa by sharp dissection tissue were flipped serosal side up and strips of the longitudinal muscle were removed by sharp dissection to reveal the underlying myenteric plexus. Colonic preparations were pinned tightly, serosal side up, in a Sylgard-lined chamber. Tissues were then loaded with the fluorescent Ca²⁺ indicator Fluo-4AM (ThermoFisher Scientific; 5 μ M) and Cremophor EL (Fluka Chemika, Buchs, Switzerland; 0.00001%) in Krebs solution at room temperature for 20 minutes with continuous oxygenation. After loading, tissues were washed (2x10 min, Krebs) prior to imaging. Subsequently, the myenteric plexus was identified and live fluorescence imaging was performed on an Olympus BX51 microscope equipped with a 20x water dipping lens (XLUMPlanFL N, NA 1, Olympus Europa), and an EMCCD camera (iXon Ultra 897, Andor Technology). Fluo-4 was excited at 470nm using an OptoLED (Cairn Research Limited), and fluorescence emission was collected at 525/50nm. Images (512X512 pixels²) were acquired at 2 Hz. Electrical train stimulation (2 s, 20 Hz of 300 μ s electrical pulses; Electronic stimulator 1001, AD instruments) was applied via a platinum/iridium electrode (tip diameter 2-4 μ m, World Precision Instruments), placed directly onto internodal strands

within the presumptive myenteric plexus the at a distance of 200 μ m from the center of the field of view. Electrical point stimulation was applied as described above, and images were collected using OptoFluor software (Cairn Research Limited). Post-acquisition analysis was performed in FIJI.³⁵ Movement artefacts were removed by registering the image stack to the first image using the StackRef plugin.³⁶ Regions of interest (ROI) of approximately 25 μ m² were drawn on ganglia-like structures or interganglionic strands within the presumptive myenteric plexus. Subsequently, fluorescence intensity was normalised to basal fluorescence for each ROI ($\Delta F/F_0$), and peaks analysed. To evaluate statistical differences between groups 5 ROI's, chosen at random from across the presumptive myenteric plexus, were analysed from each individual fetal colon sample. Final images were constructed using FIJI software.³⁵

RNA sequencing analysis

CLC-Bio (Qiagen, Venlo, The Netherlands) was used for subsequent quality control assessment, read trimming, alignment to the NCBI v37 H. sapiens reference genome, transcript quantification and differential expression analysis. Reads were aligned using the following settings: mismatch cost 2, insertion/deletion cost 3, length fraction 0.8, similarity fraction 0.8, alignment to gene regions only. Paired reads were counted as one. Trimmed mean of M values^{38,39} was used to normalize for sequencing depth across samples. Counts per Million (CPM) values were calculated for each gene, centered and scaled to unit-variance. Expression values were counted as total counts and Reads Per Kilobase of exon model per Million mapped reads (RPKM).⁴⁰ RPKM values were used for sample gene expression comparison and pathway enrichment analysis. Differential expression was calculated between groups, using the individual replicates per time-point as a group. The CLC-BIO Generalized Linear Model and Wald test were used as a statistical model to test between groups.

Candidate gene expression evaluation

Two types of output were generated. One in which reads were allowed to map to more than one location (lenient analysis) and another in which we only allowed uniquely mapped reads (stringent analysis). Lenient analysis was used for differential analysis and stringent alignment was used to validate the specificity of the expression of paralogous genes of interest (Sodium Voltage-Gated Channel Alpha Subunits, Sodium Channel Epithelial Beta Subunits, Synapsins and Semaphorins). When evaluating expression, we considered a gene to be “expressed” if it had an average CPM value of ≥ 2 for all genes across triplicates, “uncertain” when CPM values were between 1 and 2 and “not expressed” if the average CPM value was below 1. If embryological stages differed significantly ($FDR \leq 0.05$), we considered the direction of the change to be true, if not we could not determine the directionality of the change using RNA-sequencing. Raw data and the output of the lenient and stringent alignments, including CPM, total counts, RKPM, TPM and statistics are available at the Gene Expression Omnibus database (<https://www.ncbi.nlm.nih.gov/geo/>), under the accession number GSE111307.

Causal network analysis using IPA[®]

Differently expressed genes ($FDR \leq 0.05$) with a fold change ≥ 1.5 and a RPKM group mean >1 were uploaded to Ingenuity Pathway Analysis (Qiagen, Venlo, The Netherlands) for downstream pathway analysis. The causal networks analysis algorithm embedded in the Ingenuity Pathway Analysis tool was used to infer cause–effect relationships from the gene expression data results.⁴¹ As thresholds for significance we used a P value ≤ 0.05 and a Z-score of 2.